A laminar swirling jet impingement on to an adiabatic wall

Effect of inlet velocity profiles

S.Z. Shuja and B.S. Yilbas
King Fahd University of Petroleum and Minerals, Dhahran, Saudi Arabia

Received September 2000
Accepted January 2001

Keywords *Laminar flow, Flow, Velocity*

Abstract *A laminar swirling jet impinging on to an adiabatic solid wall is investigated. The flow field is computed and entropy analysis is carried out for different flow configurations. The numerical scheme employing a control volume approach is introduced when solving the governing equations of flow and energy. In order to examine the effect of the nozzle exit velocity profile and the swirling velocity on the flow field and entropy generation rate, six nozzle exit velocity profiles and four swirl velocities are considered. It is found that the influence of swirl velocity on the flow field is more pronounced as the velocity profile number reduces. In this case, two circulation cells are generated in the flow field. The total entropy generation increases with increasing swirl velocity for low velocity profile numbers. The Merit number improves for low swirling velocity and high velocity profile numbers.*

Nomenclature

a = Area
A = Nozzle exit area
Ap = Coefficient for ϕ in the numerical expression
$d\theta$ = Angular increment
h = Enthalpy
$\dot{I}$ = Irreversibility rate
k = Thermal conductivity
$\dot{m}$ = Mass flow rate
M = Merit number
n = Velocity profile number
p = Pressure
$\dot{Q}$ = Heat transfer rate
r = Distance in the radial direction
r_o = Radius of the nozzle exit
Re = Reynolds no.
S_ϕ = Source term for variable ϕ
S'''_{gen} = Volumetric entropy generation rate
$\dot{S}_{gen}$ = Integrated entropy generation rate
T = Temperature
T_{amb} = Ambient or reference temperature
T_{jet} = Jet temperature
$\forall$ = Volume
V = Velocity in the radial direction
W = Velocity in the axial direction
$\overline{W}$ = Mean velocity in the axial direction

Greek

Γ_ϕ = Exchange coefficient for ϕ
μ = Dynamic viscosity
ρ = Density
σ = Prandtl number
ϕ = Arbitrary variable
Φ = Viscous dissipation

Subscript

amb = Ambient
in = Conditions at inlet
jet = Conditions at jet
max = Maximum

The authors acknowledge the support of King Fahd University of Petroleum and Minerals, Dhahran, Saudi Arabia, for this work.

Introduction

Impinging fluid jets find wide application in industry, since they can provide very high heat and mass transfer rates. The circular jet receives considerable attention in industry due to its ease of generation and operation. The use of a single circular jet results in a localized high heat transfer rate in the stagnation region, provided that the jet exiting velocity profile influences the heat transfer characteristics. Moreover, the heat transfer rates in the stagnation region are improved by introducing the swirling in the jet flow. In this case, it results in the circulation cell being close to the stagnation region, which in turn enhances the heat transfer rate in this region.

Considerable research studies on jet impingement were carried out. Three-dimensional laminar impinging jets were simulated by Sezai and Mohamed (1999), and flow structure and heat transfer characteristics were analyzed. They indicated that the existence of streamwise velocity off-center peaks near the impingement plate was apparent. A study of the enhancement of the convection heat transfer of a laminar slot jet impinging on a porous block mounted on a heated region was investigated by Fu and Huang (1997). They showed that the heat transfer was mainly affected by a fluid flowing close to the heated region. The heat transfer for confined impinging jet on to a spherically concave surface with piston cooling application was investigated by Yang *et al.* (1999). They demonstrated the evolution of flow structure from separation point into laminar and then turbulent annular flow along the spherically concave surface. The flow and heat transfer characteristics of a submerged air jet impinging on a horizontal flat surface were studied by Siba *et al.* (1998). They indicated that two regions with distinct flow characteristics were observed:

(1) the impingement or stagnation region; and

(2) the wall jet region.

The swirling jet flow generates a recirculation zone and standing recirculating cells in the near wake region of the flow, which in turn enhances the heat transfer characteristics of the impinging surface. Recirculation zones of unconfined and confined annular swirling jets were investigated by Sheen *et al.* (1996). They indicated that the recirculation zones for both the unconfined and confined cases could be classified into seven typical flow patterns based on the Reynolds number and swirl number.

The entropy generation in a flow system is the measure of the irreversibility associated with the system. Consequently, minimizing the entropy generation enhances the available energy in the system. Considerable research studies were carried out to determine the entropy generation in the various thermal systems. The entropic efficiency of energy systems was investigated by Arpaci and Selamet (1992). They showed that the dimensionless entropy number was inversely proportional to the Peclet number in the combustion system. The second law analysis of combined heat and mass transfer in internal and external flows was studied by Carrington and Sun (1992). They indicated that assumption of thermodynamic equilibrium gave rise to errors in the analysis due to incorrect usage of the absolute mass flux instead of the diffusion flux and the appearance of

a spurious coupling term between heat and mass transfer. Bejan (1979) investigated the entropy generation in fundamental convective heat transfer processes. He suggested that, while seeking to minimize the destruction of available work in complex heat transfer equipment, it was necessary to start with optimizing the simplest design features such as the geometry of internal and external surfaces engaged in convective heat transfer. The entropy analysis of the isothermal jet was carried out by Bejan (1990). He demonstrated that the natural shape of the velocity and temperature profiles of the jet was the one that minimized the total entropy generation rate. The conjugate heat transfer from a finite thickness plate to a laminar confined, impinging planar jet was investigated by Ruocco (1997) to determine the solid-fluid coupling characteristics, which minimized the rate of entropy generation. He showed that the integrated entropy generation rate increased with the thermal conductivity ratio, whereas the plate length-averaged Nusselt number did not depend on the thermal conductivity ratio when the coolant was air. The local entropy generation in an impinging jet was investigated by Drost and White (1991). They showed that the viscous dissipation contribution of local entropy generation differed considerably for helium and glycerin in the region close to the stagnation point. They mentioned that these differences in the viscous dissipation fields were attributed to the differences between jet Reynolds numbers and fluid properties. Shuja *et al.* (2000) investigated the entropy generation in the stagnation region of the impinging turbulent jet, employing various turbulence models. They indicated that the total entropy generation differed for each turbulence model and the minimum entropy concept alone was not sufficient to assess the most appropriate turbulence model, describing the flow field in simulations.

In the present study, the flow field and entropy generation rate due to impinging laminar swirling jet are examined. In order to investigate the effect of nozzle exit jet velocity profiles on the entropy generation rate, six jet velocity profiles and four swirl velocities are considered provided that the mass flow rate and Reynolds number of the jet are kept constant in the simulations.

The mathematical model

Flow and energy equations

The axisymmetic flow condition is considered and the set of partial differential equations governing a steady flow field with constant swirl can be written in cylindrical polar coordinates as:

$$\frac{\partial}{\partial z}\left(\rho U\phi - \Gamma_\phi \frac{\partial \phi}{\partial z}\right) + \frac{1}{r}\frac{\partial}{\partial r}\left(\rho r V\phi - \Gamma_\phi r \frac{\partial \phi}{\partial r}\right) = S_\phi \qquad (1)$$

where ϕ is a general variable, Γ_ϕ is the exchange coefficient for the property ϕ, S_ϕ is the source expression for ϕ. In the most general form, it may comprise a term for the rate of generation of ϕ per unit volume together with other terms that cannot be included in terms on the left hand side of equation (1).

Equation (1) becomes the conservation for mass, axial momentum, radial momentum, tangential momentum and energy equations when setting

$\phi = 1, W, V, U$ and T respectively. Equation (1) is the compactly represented elliptic partial differential equation, and the list of the dependent variables and the associated definitions of Γ_ϕ and S_ϕ ais given in Table I.

Boundary conditions
Inlet to control volume: ($z = 0$; and $0 \leq r \leq r_0$)

$$U_{\text{in}} = \text{specified}, \ \overline{W}_{\text{in}} = \text{specified} \qquad \text{and} \qquad T_{\text{in}} = \text{specified} \tag{2}$$

Since the mass flow rate is kept constant during the simulations, the mean jet velocity in the axial direction at inlet to the control volume $(\overline{W}_{in})$ is kept constant. The velocity profile exiting the nozzle and entering the control volume is considered as:

$$W_{\text{in}} = W_{\max}[1 - (\frac{r}{r_o})]^n$$

where r_o is the nozzle exit diameter and $W_{\max}$ is the maximum axial velocity component at the nozzle exit. The mean velocity of the flow at nozzle exit can be determined from the constant volume flow rate as:

$$\overline{W_{\text{in}}} = \frac{1}{A}\int_0^{r_o} 2\pi r W_{\max}[1 - (\frac{r}{r_o})]^n dr$$

where n is the velocity profile number (and its values are given in Table II), and A is the nozzle exit area (πr_o^2).

Conservation of	ϕ	Γ_ϕ	S_ϕ
Mass	1	0	0
Axial momentum	W	μ	$-\frac{\partial p}{\partial z} + \frac{\partial}{\partial z}\left(\mu\frac{\partial U}{\partial z}\right) + \frac{1}{r}\frac{\partial}{\partial r}\left(r\mu\frac{\partial V}{\partial z}\right)$
Radial momentum	V	μ	$-\frac{\partial p}{\partial r} + \frac{\%\partial}{\partial z}\left(\mu\frac{\partial W}{\partial z}\right) + \frac{1}{r}\frac{\partial}{\partial r}\left(r\mu\frac{\partial V}{\partial r}\right) - 2\mu\frac{V}{r^2} + \rho\frac{U^2}{r}$
Tang. momentum	U	μ	$-\left(\frac{\mu}{r^2} + \rho\frac{V}{r} + \frac{1}{r}\frac{\partial\mu}{\partial r}\right)U$
Temperature	T	μ/σ	$\mu\Phi$

Table I.
Variables and the corresponding conservation equations

n	U (m/s)
1	0.01
1/1.5	0.02
1/2	0.03
1/5	
1/7	0.04
1/10	
1/200	

Table II.
Velocity profile numbers and swirl velocities used in the simulation

Outlet to control volume: ($z = 0, r_0 < r \leq 0.15$ and $0 \leq z \leq 0.05, r = 0.15$)
It is considered that the flow extends over a sufficiently long domain; therefore, it is fully developed at the exit section. Thus, for a variable ϕ the condition is:

$$\frac{\partial(r\phi)}{\partial x} = 0 \tag{3}$$

where x is the arbitrary outlet direction.

Symmetry axis: ($0 \leq z \leq 0.05$ and $r = 0$)
The radial derivative of the variables is set to zero at the symmetry axis, i.e.:

$$\frac{\partial \phi}{\partial r} = 0 \text{ and } V = 0. \tag{4}$$

Solid wall-fluid interface: ($z = 0$ and $0 < r \leq 0.15$)

The adiabatic solid wall is assumed, i.e.:

$$k_{\text{gas}} \frac{\partial T_{w_{\text{gas}}}}{\partial z} = 0$$

No slip condition is considered at the solid wall, i.e.:

$$W = V = U = 0$$

Entropy, irreversibility and heat transfer analysis
The non-equilibrium process of exchange and momentum transfer within the fluid and at the solid boundaries results in continuous entropy generation in the flow system. The local entropy generation rate per unit volume for an incompressible Newtonian fluid may be written as (Bejan, 1995):

$$S'''_{\text{gen}} = \frac{k}{T^2}(\nabla T)^2 + \frac{\mu}{T}\Phi \tag{5}$$

or

$$\left(S'''_{\text{gen}}\right)_{\text{cond}} = \frac{k}{T^2}(\nabla T)^2 \text{ and } \left(S'''_{\text{gen}}\right)_{\text{fric}} = \frac{\mu}{T}\Phi$$

where in polar coordinates;

$$\Phi = 2\left[\left(\frac{\partial V}{\partial r}\right)^2 + \left(\frac{V}{r}\right)^2 + \left(\frac{\partial W}{\partial z}\right)^2\right] + \left(\frac{\partial U}{\partial z}\right)^2 + \left(\frac{\partial V}{\partial z} + \frac{\partial W}{\partial r}\right)^2 + \left(\frac{\partial U}{\partial r} - \frac{U}{r}\right)^2$$

Here, $\left(S'''_{\text{gen}}\right)_{\text{cond}}$ represents the entropy generation per unit volume due to heat transfer and $\left(S'''_{\text{gen}}\right)_{\text{fric}}$ is the entropy generation per unit volume due to fluid friction.

The total entropy generation rate over the volume can be written as:

$$\dot{S}_{\text{gen}} = \oint_{\forall} S'''_{\text{gen}}\, d\theta\, dz\, r dr$$

where $\forall$ is the volume. The rate of total irreversibility is defined as:

$$\dot{I} = T_{\text{amb}} \dot{S}_{\text{gen}}$$

The heat transfer rate to the fluid can be written as:

$$\dot{Q} = \dot{m}_{\text{in}} C_p \left(T_{\text{jet}} - T_{\text{amb}}\right) = \dot{m}_{\text{jet}} C_p \left[T_{\text{jet}} - T_{\text{amb}}\right]$$

where $\dot{m}_{\text{jet}} = \int_0^{r_o} \rho_i W_i 2\pi r dr$. The rate of exergy transfer accompanying energy transfer at the rate of $\dot{Q}$ is given as (Mukherjee *et al.*, 1987):

$$\dot{Q}_a = \dot{Q}\left(1 - \frac{T_{\text{amb}}}{T_{\text{jet}}}\right)$$

where T_{amb} is the ambient or reference temperature, which is considered exergy reference environment temperature and T_{jet} is the jet temperature at nozzle exit.

The Merit number is defined as the ratio of exergy transferred to the sum of exergy transferred and exergy destroyed (Mukherjee *et al.*, 1987), i.e.:

$$M = \frac{\dot{Q}_a}{\dot{Q}_a + \dot{I}}$$

or

$$M = \frac{\dot{Q}\left(1 - \frac{T_a}{T_w}\right)}{\dot{Q}\left(1 - \frac{T_a}{T_w}\right) + \dot{I}}$$

Numerical solution of governing equations

For the purpose of solution the flow domain is overlaid with a rectangular grid, as shown in Figure 1, whose intersection points (nodes) denote the location at which all variables, with the exception of the velocities, are calculated. The latter are computed at locations midway between the pressures which drive them. The grid independent tests are carried out to ensure the grid independent results; consequently, the grid size and the grid orientation giving the grid independent results are selected. The mesh used in the present study has 2,500 (50×50) node points, as shown in Figure 1.

The control volume approach is used in the numerical scheme. In this case equation (1) is integrated over the control volume, with the aid of assumptions about the relations between the nodal values at ϕ and the rates of creation/destruction of this entity within the cells and its transport by convection and

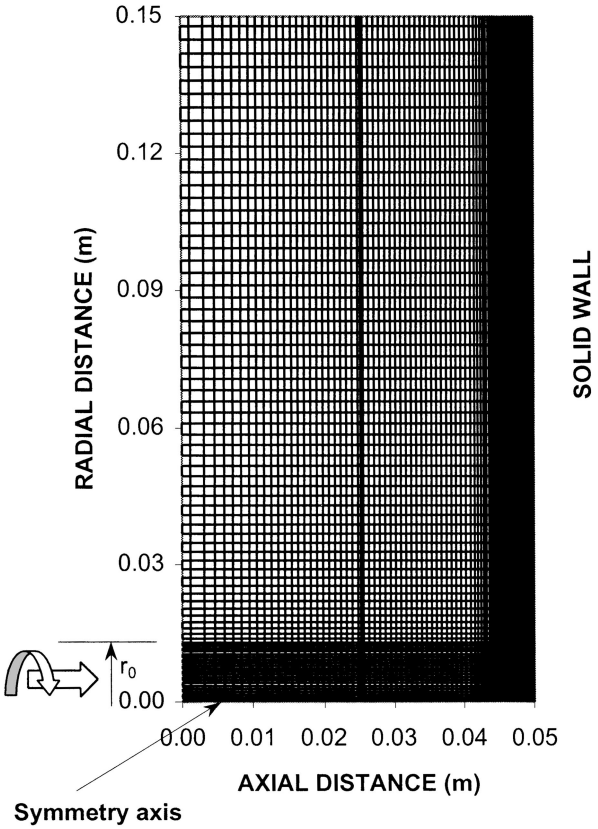

Figure 1.
Geometric layout of the solution domain and grid used in the simulations. The arrows represent the jet inlet and swirl directions, while r_0 (0.0127m) is the jet radius

diffusion across the cell boundaries. The former is represented in linearized form as:

$$S_\phi \equiv \int_{\forall} s_\phi \, d\forall = S_0 + S_P \phi_P$$

and the transport by expressions of the form:

$$\rho U_w \frac{(\phi_P + \phi_W)}{2} a_w - \Gamma_{\phi,w} \frac{(\phi_P + \phi_W)}{\delta x_{PW}} a_w$$

when the quantity Pe_w (the cell Peclet number = $\rho U_w \, \delta x_{PW} / \Gamma_{\phi,w}$) is small and by:

$$\rho U_w \phi_W \text{ if } \mathrm{U_w} > 0$$

$$\rho U_w \phi_P \text{ if } \mathrm{U_w} < 0$$

when Pe_w is large in magnitude, where subscripts P and W refer to the central and west nodes, respectively, and w denotes the intervening cell boundary. Assembly of the above and similar expressions for the remaining boundaries yield for the finite difference equation in the form:

$$(A_P - S_P)\phi_P = \sum_n A_n \phi_n + S_0$$

where $\sum_n$ is the summation over the neighboring nodes, $A_P = \sum A_n$, and S_0 and S_P are deduced from S_ϕ of Table I. The finite difference equations are written for each of the variables at every cell with appropriate modifications being made to the total flux expressions at cells adjoining the boundaries of the solution domain to take account of the conditions imposed there.

A staggered grid arrangement is used in the present study. This arrangement provides for handling the pressure linkages through the continuity equation and is known as the SIMPLE algorithm (Patankar, 1981). This method is an iterative process to steady-state convergence. The pressure link between continuity and momentum is accomplished by transforming the continuity equation into a Poisson equation for pressure. The Poisson equation implements a pressure correction for a divergent velocity field. The steady-state convergence is achieved by successively predicting and correcting the velocity components and the pressure. An initial guess for the pressure variable at each grid point is introduced.

Results and discussions

A laminar swirling jet impinging on to an adiabatic wall is considered. The nozzle to wall spacing is taken as 2, while the jet Reynolds number is kept at 50 at the nozzle exit in the simulations. The nozzle exit velocity profile is changed, while keeping the swirl velocity constant at each simulation condition. The computation is repeated for all the swirling velocities employed in the present study.

Figure 2 shows the velocity vectors for different flow configurations. In general, a circulation cell is generated away from the solid wall. The size of the circulation cell changes with different flow configurations, as can be seen from the Figure. The effect of velocity profile number (n) on the circulation cell is visible. In this case, as the velocity profile number increases, the size and speed of the circulation cell increase. This occurs because the high velocity profile number results in a triangle-like velocity profile at the nozzle exit. This increases the magnitude of the maximum velocity at the nozzle exit, since the mass flow rate is kept constant for all velocity profile numbers. Therefore, the flow after the impingement expands radially with increasing velocity. Consequently, the radial momentum changes the size of the circulation cell and increases the circulation speed. The influence of swirling on the flow field is more pronounced as the swirl velocity increases to 0.04m/s. In this case, the orientation of the circulation cell close to the solid wall changes such that it

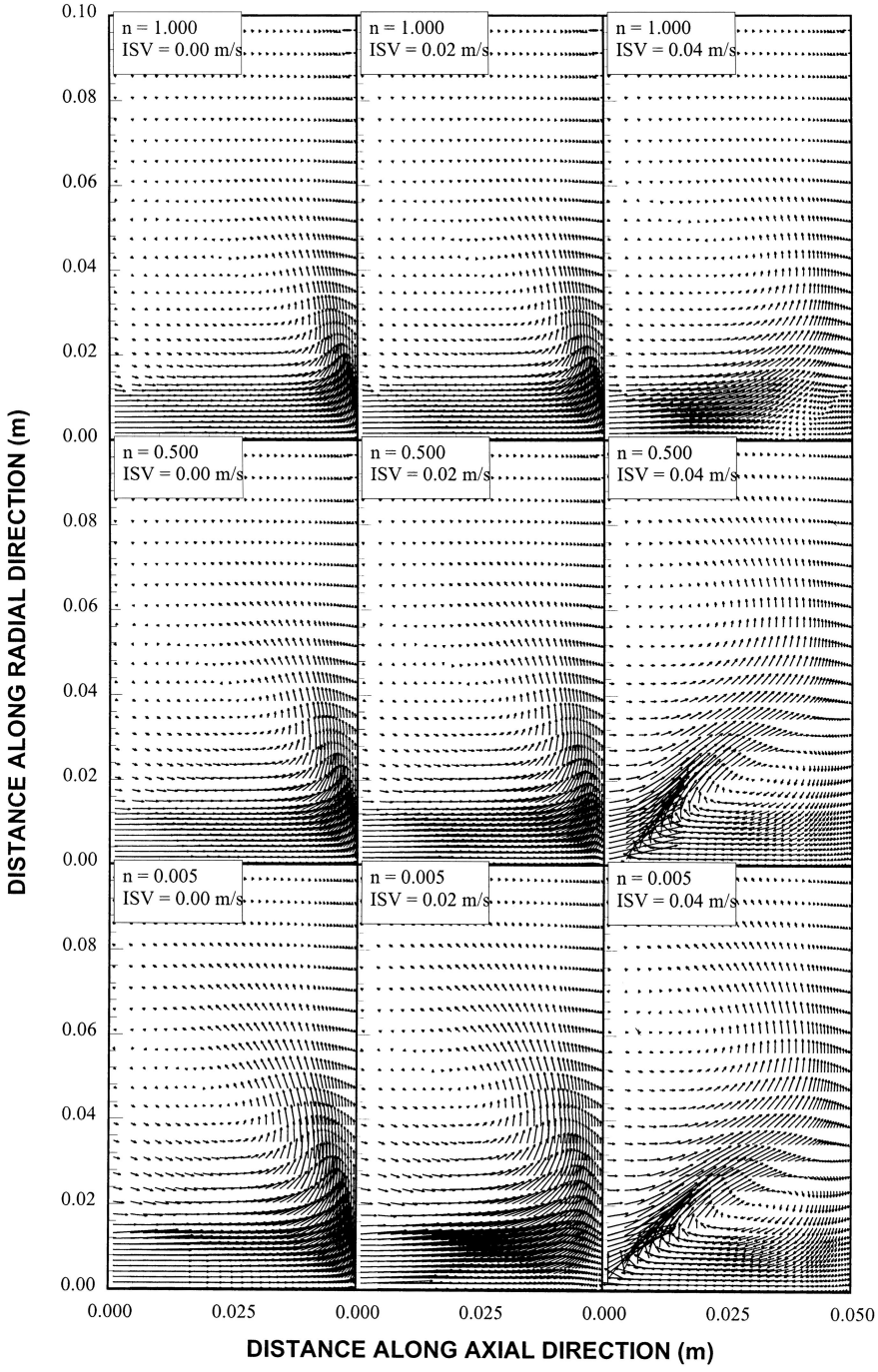

Figure 2.
Velocity vectors corresponding to different flow configurations. *n* is a velocity profile number and ISV represents inlet swirl velocity

moves slightly away from the wall and the flow speed in the circulation cell reduces considerably. The combined effect of velocity profile number and swirl velocity is more pronounced at high velocity numbers and large swirl velocity. In this case, a secondary counter-rotating cell is generated beside the first circulation cell. The generation of a secondary circulation cell shows that the jet expands as it swirls before impinging on to the wall. This is also evident from Figure 3, in which the axial velocity (W) contours for different flow configurations are shown. This enhances the radial momentum in this region, which in turn results in the development of the secondary counter-rotating cell away from the wall and close to the impinging jet. The condition corresponding to the extreme flow configuration, where the velocity profile number is 0.05 and swirl velocity 0.04 m/s, results in a relatively large secondary circulation cell next to the impinging jet.

Figure 4 shows the temperature contours for different flow configurations. The temperature contours in the stagnation region and in the far field (away from the nozzle exit) are affected by the velocity profile number. In this case, the temperature contours extend further in the far field when the velocity profile number attains high values; however, the extension of the temperature contours is limited to along the wall when the velocity profile number becomes less, i.e. uniform jet profile (n is small) improves the convective energy transport in the far field, while triangle-like velocity profile (n is large) improves the convective energy transport close to the wall. This situation almost reverses, once the swirling is introduced, i.e. the convective energy transport improves towards the far field as swirling velocity increases. The effect of the velocity profile number on the temperature contours is less significant compared with that corresponding to the swirl velocity. This is because the swirling results in expansion of the jet before it impinges on to a wall. Moreover, the coupling effect of the velocity profile number and the swirl velocity on the temperature contours is more pronounced as the velocity profile number reduces while the swirl velocity increases. This is due to the complex flow field generated for this flow configuration, i.e. two counter-rotating circulation cells alter the convective energy transport in the solution domain.

Figure 5 shows the volumetric entropy contours, including fluid friction and heat transfer contributions, for different flow configurations. The entropy generation rate increases in the region close to the nozzle exit. It is apparent that the entropy generation in the stagnation region is negligible compared with that corresponding to the nozzle exit. This is because the heat transfer contribution of the entropy generation, is almost $10^3\times$ higher than the frictional contribution of entropy generation. In this case, the temperature difference between the jet and its ambient results in a relatively high temperature gradient in the region close to the nozzle exit. Consequently, the high temperature gradient enhances the entropy generation rate (equation (5)). The effect of the velocity profile number on the entropy generation is more pronounced as the profile number increases, i.e. once the jet velocity has a triangle-like profile, the temperature gradient across the jet increases, which in turn contributes significantly to the entropy generation

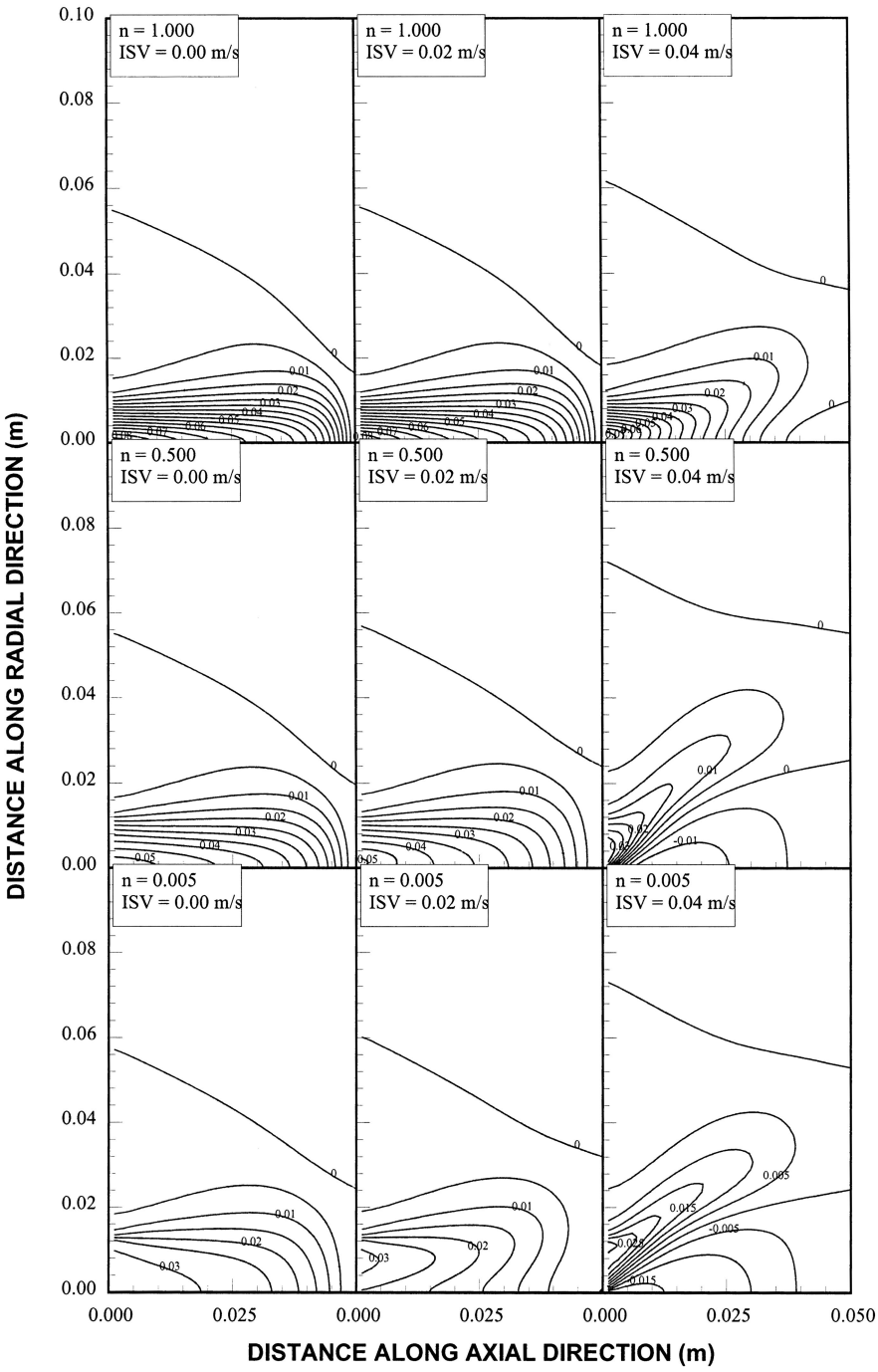

Figure 3.
Axial velocity contours corresponding to different flow configurations. *n* is a velocity profile number and ISV represents inlet swirl velocity

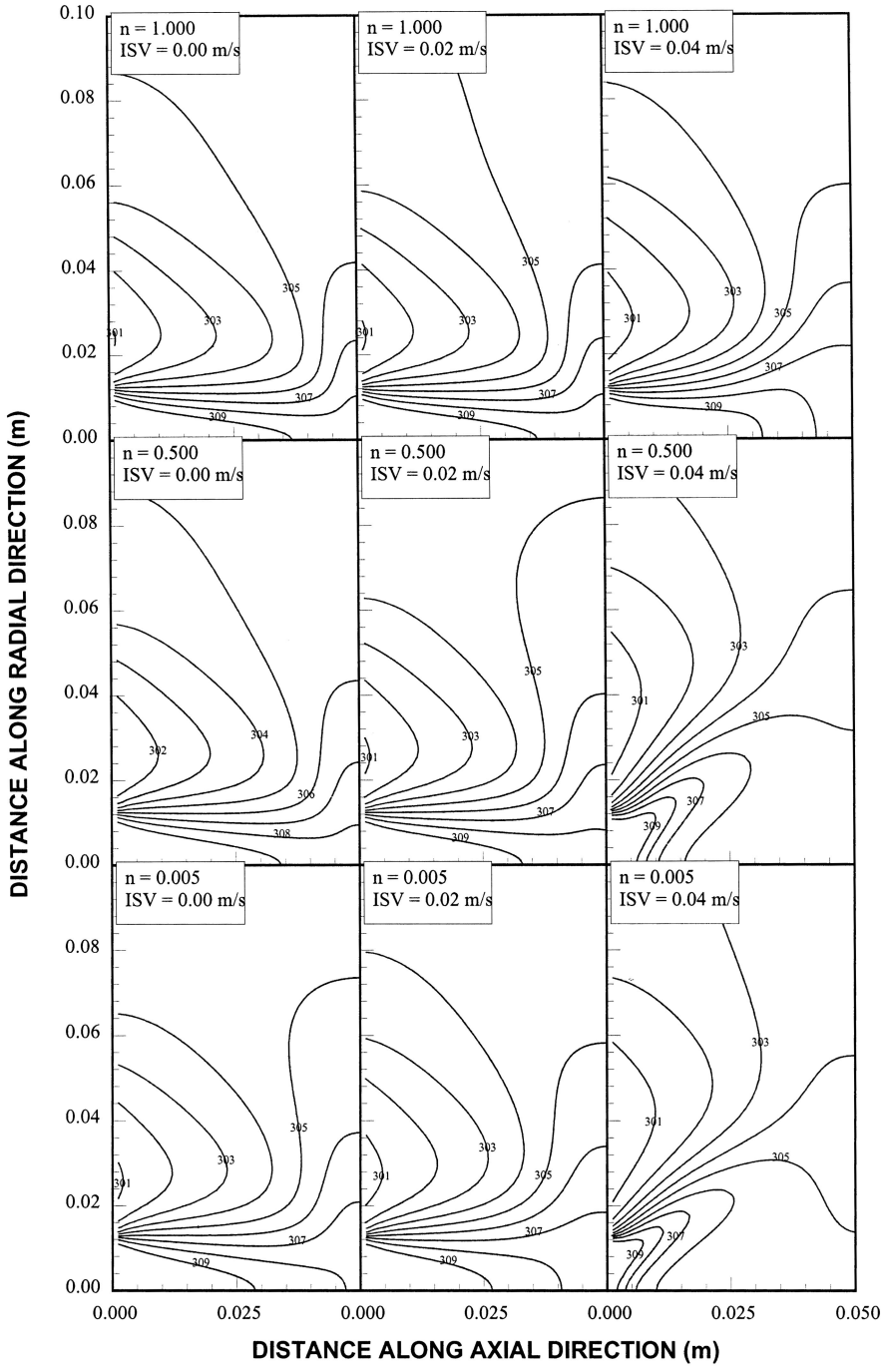

Figure 4.
Temperature contours corresponding to different flow configurations. *n* is a velocity profile number and ISV represents inlet swirl velocity

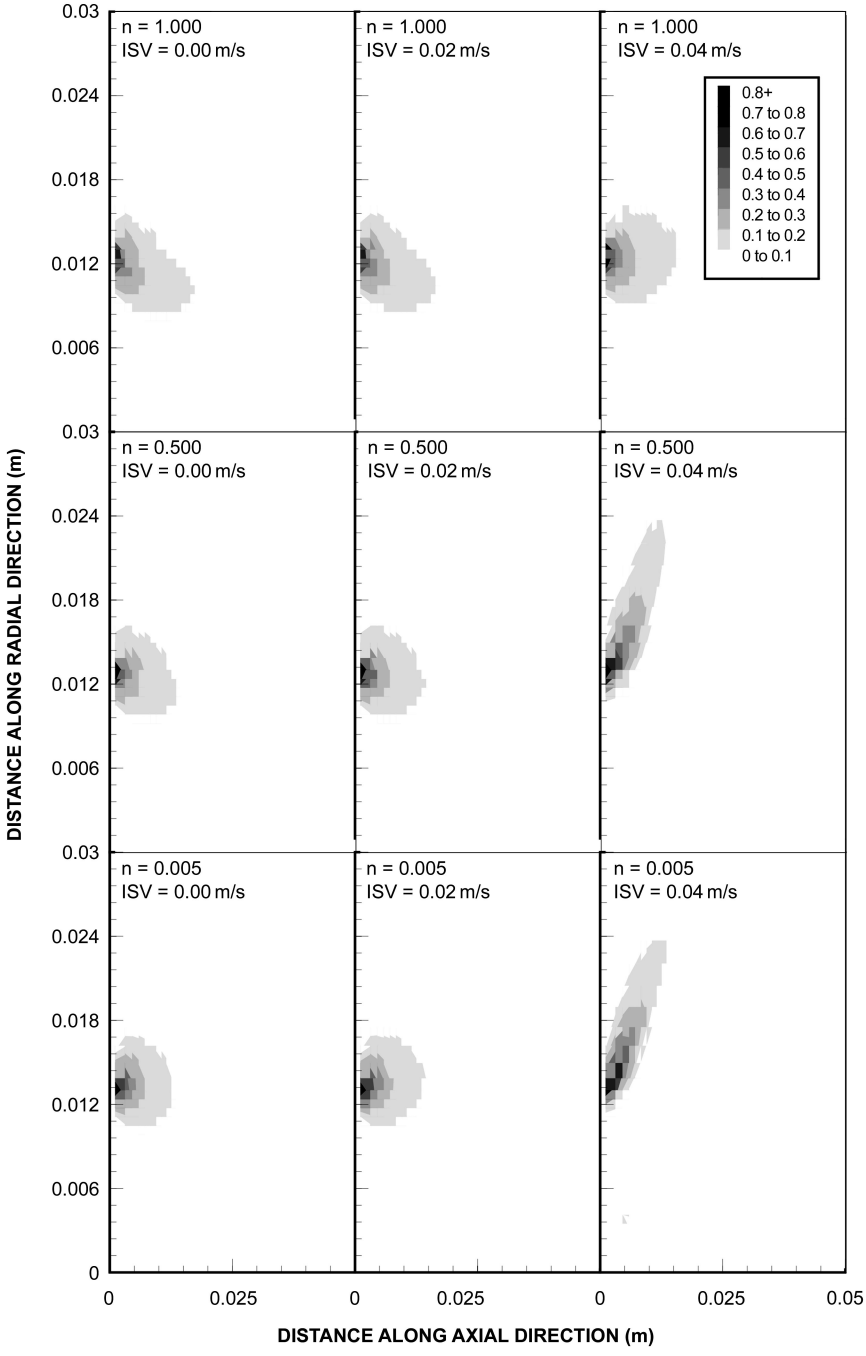

Figure 5.
Entropy contours corresponding to different flow configurations. *n* is a velocity profile number and ISV represents inlet swirl velocity

rate. The influence of swirl velocity on the entropy generation rate assumes significance as the velocity profile number reduces. In this case, the entropy contours extends towards the far field. This is due to enhanced convective energy transport towards the far field, i.e. the hot fluid is carried towards the far field and it generates a high temperature difference between the hot fluid and its ambient; therefore, the temperature gradient in the far field increases, which in turn increases the entropy generation rate.

Figure 6 shows the integrated volumetric entropy generation rate (integrated over the volume) due to fluid friction with the velocity profile number as a swirl velocity variable. The entropy generation rate increases with the velocity profile number for swirl velocities up to 0.03m/s, provided that, as the swirl velocity increases, the entropy generation rate reduces. This indicates that the viscous dissipation increases as the jet velocity at the nozzle exit tends to deviate from the uniform-like profile. In this case, the maximum velocity at the nozzle exit increases, since the mass flow rate is kept constant, and the steep change in the velocity profile results. Therefore, the viscous dissipation across the jet increases gradually as the jet velocity profile approaches a triangle-like profile. In the case of swirl velocity 0.03m/s, the entropy generation rate reduces to minimum for a velocity profile number 0.5, i.e. the viscous dissipation is minimal for this particular flow configuration. However, as swirl velocity increases further ($U = 0.04$m/s), the entropy generation rate reduces with the increasing velocity number. In this case, the flow field changes completely and large circulation cells are generated for low velocity profile numbers (see Figure 2). This contributes considerably to the entropy generation rate due to fluid friction.

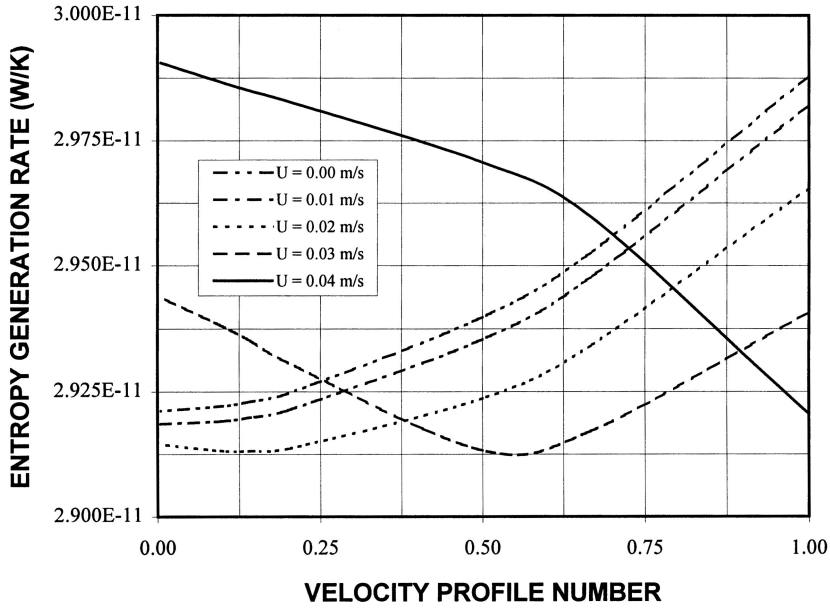

Figure 6.
Entropy generation rate due to fluid friction with velocity profile number as swirl velocity variable

Figure 7 shows the total integrated entropy generation rate (due to heat transfer and fluid friction contributions and integrated over the volume) with the velocity profile number as a swirl velocity variable. Total entropy generation rate reduces as the velocity profile number increases. This is because the entropy generation rate due to the heat transfer contribution with the increasing velocity profile number. In this case, the temperature gradient across the jet increases as the jet velocity profile takes on a uniform-like profile, i.e. a sudden jump in temperature occurs between the jet and its ambient. The effect of the swirl velocity on the total entropy generation rate is significant. The total entropy generation rate increases with increasing swirl velocity. This is more pronounced as the velocity profile number reduces. It should be noted that the contribution of heat transfer to the total entropy generation rate is significantly higher than the fluid friction contribution. The hot jet is carried towards the far field by the radial momentum at high swirl velocities, which in turn results in a large zone of non-uniform temperature region in the flow field, i.e. the high temperature gradient produces large entropy generation rates.

Figure 8 shows the Merit number variation with the velocity profile number as a swirl velocity variable. The Merit number attains relatively higher values for low swirl velocities compared with that corresponding to high swirl velocity. This indicates that the useful energy transfer rate to irreversibility rate improves as the swirl velocity reduces. The effect of the velocity profile number on the Merit number becomes more evident as the swirl velocity increases. In this case, the Merit number increases with the increasing velocity profile number, i.e. the triangle-like jet velocity profile at the nozzle exit

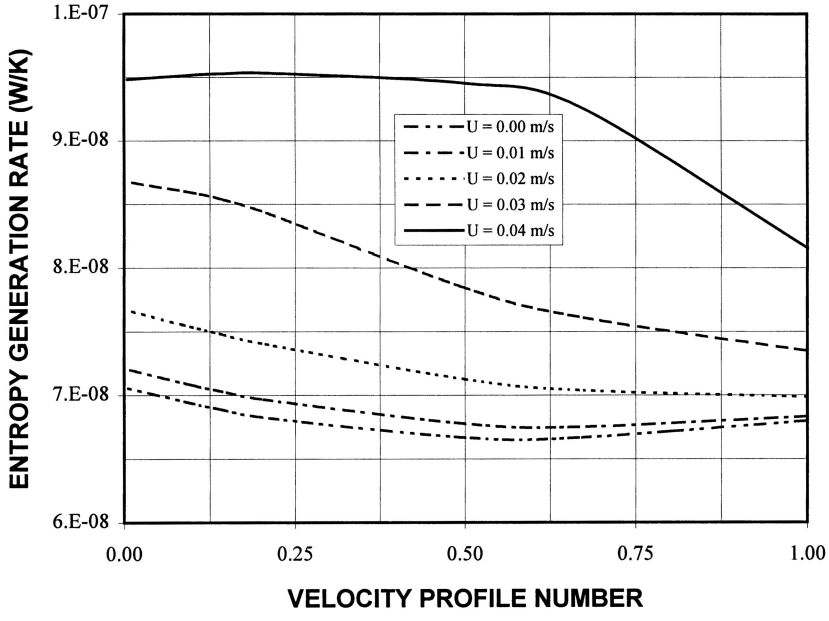

Figure 7.
Total entropy generation rate due to fluid friction and heat transfer with velocity profile number as swirl velocity variable

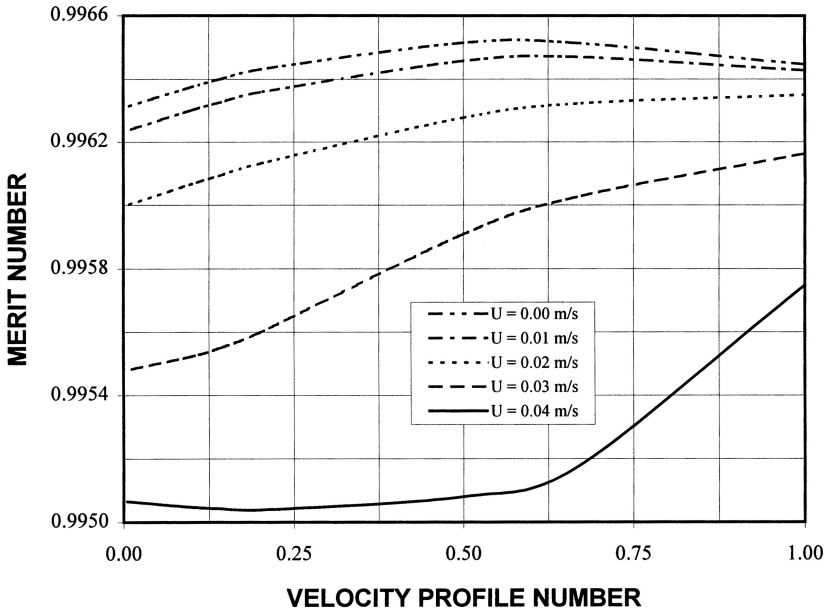

Figure 8.
Merit number with velocity profile number as swirl velocity variable

improves the Merit number. Therefore, the irreversibility rate in the flow system increases as the velocity profile approaches uniform at the nozzle exit and the velocity profile number 0.5 without swirl condition maximizes the Merit number and minimizes the irreversibility rate associated with the system. Moreover, the optimum Merit number is only extended to swirl velocity 0.01m/s, i.e. the Merit number increases continuously as the swirl the velocity increases beyond 0.01 m/s and velocity profile number increases.

Conclusions

The laminar swirling jet impinging on to an adiabatic solid wall is considered. The flow field due to different swirl velocities and jet velocity profiles at the nozzle exit is computed. The resulting entropy generation rate due to heat transfer and fluid friction contributions is computed. In general, velocity profile at the nozzle exit and swirling have a coupling effect on the flow field. In this case, as the swirl velocity increases while velocity profile number reduces, a secondary counter-rotating circulation cell next to the impinging jet is generated beside the existing circulation cell close to the wall. This results in increased total entropy generation rate in the flow field, which in turn reduces the Merit number. The specific conclusions derived from the present study can be listed as follows:

(1) The counter-clockwise circulation cell is developed in the flow field close to the solid wall for all velocity profile numbers at low swirl velocities, provided that, as the velocity profile number reduces, the orientation of the circulation cell changes and the cell moves slightly away from the

wall. In this case, the jet velocity profile at the nozzle exit approaches a uniform-like profile. When the velocity number reduces and swirl velocity increases, a secondary clockwise circulation cell is developed in the region close to the jet. Increasing swirl velocity results in a slight expansion of the jet in the radial direction.

(2) The temperature contours in the flow field extend further into the far field as the velocity profile number increases; in which case, the magnitude of maximum velocity increases. The temperature contours extend along the solid wall as the velocity profile number reduces. This situation almost reverses as the swirl velocity increases. Consequently, at high velocity profile numbers hot gas is carried further into the far field, which in turn results in a non-uniform temperature region in this region.

(3) The total volumetric entropy generation rate (including heat transfer and fluid friction contributions) reduces with increasing velocity profile number; however, it increases considerably once the swirl velocity increases. This is due to the heat transfer contribution of entropy generation, which is higher than its counterpart corresponding to fluid friction. In this case, the non-uniform temperature field results in a high temperature gradient in the large region of the flow field. The fluid friction contribution of entropy generation rate reduces to the minimum for the velocity profile number of 0.5 for no swirl condition.

(4) The Merit number improves for low swirl velocities and it reaches its maximum when the velocity profile number becomes 0.5 without swirl condition. The irreversibility rate in the flow field increases as the velocity profile number reduces, while swirl velocity becomes 0.04m/s. In this case, the Merit number attains low values.

References

Arpaci, V. and Selamet, A. (1992), "Entropic efficiency of energy systems", *Prog. Energy Combustion Science*, Vol. 18, pp. 429-45.

Bejan, A. (1979), "A study of entropy generation in fundamental convective heat transfer," *ASME, J. Heat Transfer*, Vol. 101, pp. 718-25.

Bejan, A. (1990), "Thermodynamics of an isothermal flow: the two-dimensional turbulent jet", *Int. J. Heat and Mass Transfer*, Vol. 34, pp. 407-13.

Bejan, A. (1995), *Entropy Generation Minimization*, CRC Press, New York, NY.

Carrington, G. and Sun, Z.F. (1992), "Second law analysis of combined heat and mass transfer in internal and external flows", *Int. J. Heat and Fluid Flow*, Vol. 13, pp. 65-70.

Drost, M.K. and White, M.D. (1991), "Numerical predictions of local entropy generation in an impinging jet", *ASME J. Heat Transfer*, Vol. 113, pp. 823-9.

Fu, W. and Huang, H. (1997), "Thermal performances of different shape porous blocks under an impinging jet", *Int. J. Heat and Mass Transfer*, Vol. 40, pp. 2261-72.

Mukherjee, P., Biswas, G. and Nag, P.K. (1987), "Second-law analysis of heat transfer in swirling flow through a cylindrical duct", *ASME J. Heat Transfer*, Vol. 109, pp. 308-13.

Patankar, S.V. (1981), *Computer Analysis of Fluid Flow and Heat Transfer*, Pinridge, Swansea, Chapter 8, pp. 223-52.

Ruocco, G. (1997), "Entropy generation in conjugate heat transfer from a discretely heated plate to an impinging confined jet", *Int. Comm. Heat and Mass Transfer*, Vol. 24, pp. 201-10.

Sezai, I. and Mohamed, A.A. (1999), "Three-dimensional simulation of laminar rectangular impinging jets, flow structure and heat transfer", *ASME Journal of Heat Transfer*, Vol. 121, pp. 50-56.

Sheen, H.J., Chen, W.J. and Jeng, S.Y. (1996), "Recirculation zones of unconfined and confined annular swirling jets", *AIAA Journal*, Vol. 34, pp. 572-9.

Shuja, S.Z., Yilbas, B.S. and Budair, M.O. (2000), "Local entropy generation in an impinging jet: minimum entropy concept evaluating various turbulence models", *Computer Methods in Applied Mechanics and Engineering*.

Siba, E.A., Ganesa-Pillai, M., Harris, K.T. and Haji-Sheikh, A. (1998),"Turbulent heat transfer in single phase jet impingement flow over a flat circular disk", *Proceedings of 1998 ASME Int. Mech. Eng. Congress and Exposition*, Anaheim, pp. 15-20, *ASME Heat Transfer Div. Publication*, Vol. 361, pp. 191-202.

Yang, T.L., Chang, S.W., Su, L.M. and Hwang, C.C. (1999), "Heat transfer of confined impinging jet on to spherically concave surface with piston cooling application", *JSME Int. J. Series, B*, Vol. 42, pp. 238-48.